1-2012

Ceria-Engineered Nanomaterial Distribution in, and Clearance from, Blood: Size Matters

Mo Dan
University of Kentucky, mo.dan@uky.edu

Peng Wu
University of Kentucky, peng.wu@uky.edu

Eric A. Grulke
University of Kentucky, eric.grulke@uky.edu

Uschi M. Graham
University of Kentucky, uschi.graham@uky.edu

See next page for additional authors

Ceria-Engineered Nanomaterial Distribution in, and Clearance from, Blood: Size Matters

Digital Object Identifier (DOI)
https://doi.org/10.2217/nnm.11.103

Notes/Citation Information
Published in *Nanomedicine*, v. 7, no. 1.

Authors
Mo Dan, Peng Wu, Eric A. Grulke, Uschi M. Graham, Jason M. Unrine, and Robert A. Yokel

Ceria engineered nanomaterial distribution in and clearance from blood: Size matters

Mo Dan[1,2], Peng Wu[3], Eric A. Grulke[3], Uschi M. Graham[4], Jason M. Unrine[5], Robert A. Yokel[1,2,*]

[1]College of Pharmacy, [2]Graduate Center for Toxicology,[3]Chemical & Materials Engineering, [4]Center for Applied Energy Research,[5]Plant and Soil Science, University of Kentucky, Lexington, KY

*Corresponding author:

Robert A. Yokel, Ph.D.

Department of Pharmaceutical Sciences

College of Pharmacy

511C Multidisciplinary Sciences Building

725 Rose Street

University of Kentucky Academic Medical Center

Lexington, KY, 40536-0082

phone: 859-257-4855

fax: 859-257-7585

e-mail: ryokel@email.uky.edu

Mo Dan

Department of Pharmaceutical Sciences

College of Pharmacy

541 Multidisciplinary Sciences Building

725 Rose Street

University of Kentucky Academic Medical Center

Lexington, KY, 40536-0082

phone: 859-257-2572

fax: 859-257-7585

e-mail: mo.dan@uky.edu

Peng Wu

Chemical & Materials Engineering Department

215 ASTeCC Building

University of Kentucky

Lexington, KY, 40506-0503

phone: 859- 218-6503

fax: 859-323-1929

e-mail: PENG.WU@uky.edu

Eric A. Grulke

Chemical & Materials Engineering Department

359 Ralph G. Anderson Building

University of Kentucky

Lexington, KY, 40506-0503.

phone: 859-257-6097

fax: 859-323-1929

e-mail: eric.grulke@uky.edu

Uschi M. Graham

Center for Applied Energy Research

2540 Research Park Drive

University of Kentucky, Lexington, KY, 40511

phone: 859- 257-0299

fax: 859-257-0302

e-mail: uschi.graham@uky.edu

Jason M. Unrine

Department of Plant and Soil Sciences

N212-N Agricultural Science Center North

1100 S. Limestone St.

University of Kentucky

Lexington, KY, 40546-0091

phone: 859-257-1657

fax: 859-257-3655

e-mail: jason.unrine@uky.edu

Abbreviations:

Alpha (α)	initial half-life in a two compartment model, usually representing distribution
AUC	area under the curve
Beta (β)	second decay half-life in a two compartment model, usually representing elimination
Ce	cerium
CL	clearance
C_{max}	maximum concentration
ENM	engineered nanomaterial
iv	intravenous
ICP-MS	inductively coupled plasma mass spectrometry
MDL	method detection limit
MRT	mean residence time
PBPK	physiologically-based pharmacokinetic
$t_{½}$	half-life
Vd_{ss}	apparent volume of distribution at steady state

Abstract:

Objectives: Characterize different sized ceria engineered nanomaterial (ENM) distribution in and clearance from blood, compared to the cerium ion, following intravenous infusion. **Methods:** Cerium (Ce) was quantified in whole blood, serum, and clot (the formed elements) up to 720 h. **Results:** Traditional pharmacokinetic modeling showed best fit for 5-nm ceria ENM and the cerium ion. Ceria ENMs larger than 5 nm were rapidly cleared from blood. After initially declining, whole blood 15- and 30-nm ceria increased; results not well-described by traditional pharmacokinetic modeling. The cerium ion and 5- and 55-nm ceria did not preferentially distribute into serum or clot, a mixture was predominantly in the clot, and 15- and 30-nm ceria migrated into the clot over 4 h. **Conclusions:** Five-nm ceria may not be readily recognized by reticuloendothelial organs. Increased ceria distribution into the clot over time may be due to opsonization. Traditional pharmacokinetic analysis was not very informative. Ceria ENM pharmacokinetics are quite different from the cerium ion.

Key words:

blood, ceria, distribution in blood, engineered nanomaterial, half-life, pharmacokinetics, systemic clearance

Future perspective:

Current uncertainties in nanoscale material evaluation in biological systems include proper/adequate material characterization, the dose metric(s) that best describe and predict their effects, and whether they behave like traditional xenobiotics. A key component of research quality and standardization with nanoscale materials is their physicochemical characterization. The “appropriate” characterization methods are currently under intense debate, as is the “best” metric of dose or exposure. Further research results that identify the material characterization methods most relevant to their biological properties and dose metrics that best predict ENM response will guide researchers toward more standard and appropriate methods, increase confidence in the results, and generate more consistent results. This is occurring and is expected to mature in the next 5 to 10 years.

The ongoing generation of research results by many groups describing the kinetics of ENMs will provide much more insight into how ENMs are handled *in vivo*. The kinetic endpoints include absorption (uptake), distribution, biotransformation (and opsonization), re-distribution (translocation), and elimination. These appear to be greatly influenced by the physicochemical properties of nanoscale materials. As noted in a recent review of the pharmacokinetics of carbon-based and quantum dot ENMs, they are not amenable to classical pharmacokinetic parameter estimations due to their differences from the solution chemistry of their components. Results of the present work support this observation, leading to the necessity to adopt or develop other approaches to describe ENM pharmacokinetics. It is anticipated that this will occur over the next 5

to10 years, perhaps utilizing predictive, pharmacokinetic, physiologically-based, or non-traditional modeling approaches. This study illustrates the necessity of developing such models.

Executive summary:

- Nanoscale ceria pharmacokinetics, biodistribution, and clearance pattern cannot be predicted from those of the cerium ion.
- Nanoscale ceria circulation time in the blood of particles too large to be filtered by the kidney (> 5 nm) and apparently too small to be readily recognized by the reticuloendothelial organs (< 15 nm) is much longer than larger nanoscale ceria.
- Cubic and polyhedral nanoscale ceria that was 15 nm or greater in diameter was very rapidly cleared from circulating blood. The small remaining fraction in blood persisted for some time.
- Nanoscale ceria size and shape influenced its distribution between blood serum compared to a blood fraction containing red cells, white cells, and platelets.
- The results suggest nanoscale ceria undergoes surface chemistry changes in blood within hours of its entry, and that these changes are most pronounced with 15 to 30 nm ceria particles. This may be due to opsonization.
- The sites of ceria ENM residence in and outside of circulating blood during the first several hours after its administration and the physicochemical properties that influence this are not well understood.
- A firm understanding of the rate and nature of ceria ENM association with blood proteins and cells and the process(es) of their clearance from blood are needed to fully interpret their fate in the vascular compartment.
- The analysis of nanoscale particle concentration in blood vs. time is not amenable to traditional pharmacokinetic analyses. This is illustrated by the increase in cerium in blood after ceria ENM iv infusion; an unusual property

following the iv administration of agents. Non-classical methods are necessary to model and interpret the pharmacokinetics of ENMs.

Introduction:

There has been much research to develop engineered nanomaterials (ENMs). Polymer ENMs are being developed as drug delivery systems [1, 2], and some metal and metal oxide ENMs are being developed as therapeutic agents. Human exposure may also come from occupational and environmental sources. Little is known about ENM distribution or persistence in the vascular system. We were unable to find published studies of the distribution of metal or metal oxide ENMs among blood compartments.

To investigate the persistence and distribution of a model ENM in blood we utilized ceria (a.k.a.: CeO_2, ceric oxide). Numerous studies reported ceria ENM to be neuro- and cardioprotective, suggesting it has therapeutic utility in medical disorders caused by reactive oxygen species [3-11]. On the other hand, there are reports of ceria-induced toxicity associated with increased oxidative stress [12-17]. Nanoscale ceria is a catalyst, marketed as a diesel fuel additive, generated during combustion in the Eolys® system [101], and is in the walls of self-cleaning ovens. As an abrasive it is used in chemical-mechanical planarization in electronic circuit manufacture. Nanoscale ceria was nominated by the U.S. National Institute for Environmental Health Sciences, NIH, for toxicological consideration, including toxicokinetic studies [102]. The Organisation for Economic Co-operation and Development Environment Directorate included ceria on its priority list of nanomaterials in commerce (or likely to enter into commerce in the near term) for measurement, toxicology and risk assessment [103]. However, there are no reported studies of the pharmacokinetics of nanoscale ceria other than our report that a commercial ~ 30-nm ceria had an initial $t_{½}$ of ~ 0.125 h [18]. It is vitally important to

understand the pharmacokinetics of ENMs in relation to their potential therapeutic applications and/or toxicity. The pharmacokinetics of carbon-based ENMs and quantum dots has been reviewed [19], but much less has been reported for other metal and metal oxide ENMs.

Little is known about the influence of size on the distribution in and clearance from blood of metal and metal oxide ENMs. We found that the blood cerium concentration was 0.56 and 1.3 mg/L after a 1 h infusion of 50 or 250 mg/kg of an ~ 30-nm commercial ceria ENM to rats [18]. In contrast, 1 h after infusion of 100 mg/kg of an in-house manufactured 5-nm ceria ENM it was 370 mg/L [20], suggesting that the rate of metal oxide ENM clearance from blood was size dependent. The present study was conducted to test this hypothesis.

Another factor that influences the rate of ENM clearance from blood and their distribution is their surface chemistry, including charge and surface coating. A zeta potential greater than +30 or less -30 mV decreases the potential for agglomeration in the medium due to repulsive electrostatic forces [21]. ENMs are often coated with polymers such as polyethylene glycol or oxygen-rich ions such as citrate. These coating increase ENM hydrophilicity and stabilize ENM dispersions through the electrostatic repulsion mechanism, which may reduce their clearance by the reticuloendothelial system [22-25]. [Note: do not use the work, solubility, here.]Citrate, an endogenous molecule present in the blood and an integral component of the tricarboxylic acid cycle, was used in the present study as a ceria surface coating to minimize agglomeration. It

has been shown that citrate-surface coating of metal/metal oxide ENMs resulted in their non-specific attachment to the surface of HeLa cells *in vitro* and over-coating by humic acid and albumin [24, 26, 27].

The present work was conducted to test the hypotheses that the fate of a metal oxide ENM in blood is different than its constituent metal and that ENM size and shape influence its persistence in and distribution within the major components of blood. We iv infused the cerium ion, four sizes of cubic or polyhedral citrate-coated ceria ENMs, and a mixture of cubic and rod-shaped ceria to rats. Blood was repeatedly withdrawn up to 4 h later, and in some cases up to 30 days. An aliquot of each blood sample drawn up to 4 h after ceria infusion was allowed to clot. By comparison of Ce in whole blood, serum, and the clot we could determine pharmacokinetic parameters of ceria distribution in, and clearance from, blood.

Materials and methods:

Cerium chloride heptahydrate (Sigma-Aldrich #228931, 99.9% metal basis), cerium nitrate hexahydrate (Sigma-Aldrich # 22350, >99.0%), sodium hydroxide (Fisher #S318-1, certified ACS pellets), ammonium hydroxide (Fisher # 3256, ACS, 28-30%), hexadecyltri-methylammonium bromide (CTAB, Sigma-Aldrich #H9151, ~99.0%), deionized ultra filtered water (DIUF, Fisher #W2-20), and citric acid monohydrate (EMD Chemicals Inc # CX1725-1, GR ACS) were used without further purification.

Ceria ENM synthesis

Five nm ceria ENM was synthesized as described [28]. Typically a 20 ml aqueous mixture of 0.5 M (0.01 mol) ceria chloride and 0.5 M (0.01 mol) citric acid was added to 20 ml of 3 M ammonium hydroxide. The latter was in excess of that needed for complete reaction of the cerium chloride to cerium hydroxide. The final product was an un-buffered ceria dispersion with a pH of 8 to 9. After stirring for 24 h at 50°C, the solution was transferred into a Teflon-lined stainless steel bomb and heated at 80°C for 24 h to complete the reaction. The cerium concentration in samples taken from the top and bottom of two ceria dispersion samples that were un-disturbed for > 2 months were within 2.5% of each other, demonstrating dispersion stability. Settling of the 5 nm ceria dispersion was not observed over at least three months and dynamic light scattering estimates of 5 nm ceria particle size distributions were similar to those obtained initially. The dispersed ceria ENM was infused intravenously without any further treatment.

Fifteen nm ceria ENM was synthesized using a hydrothermal procedure [29]. In a typical procedure, 2 ml ammonium hydroxide was drop-wise added into 20 ml aqueous mixture of 1.5 mmol cerium nitrate and 0.5 mmol CTAB and kept stirring for 0.5 h to form a brown emulsion. The emulsion was transferred into a Teflon-lined stainless steel bomb and heated at 120 °C for 24 h to complete the reaction. The fresh product was washed with water three times to remove free cerium, dialyzed three times with fresh citric acid aqueous solution, and dried at 55 °C for 24h. The final 15 nm citrate modified ceria powder was re-dispersed into water to prepare a ~5 wt% aqueous suspension. The pH of the resulting un-buffered ceria dispersion was 3.5.

Thirty nm ceria was synthesized using a hydrothermal approach [30]. Generally, 20 ml aqueous mixture of 1 mmol cerium nitrate and 105 mmol sodium hydroxide was stirred for 0.5 h to get a milky suspension. The suspension was transferred into a Teflon-lined stainless steel bomb and heated at 180 °C for 24 h. After the hydrothermal treatment, fresh white precipitates were washed with deionized water three times and then ethanol three times to remove the free cerium and organic impurities. Then the wet precipitates were dispersed into 0.05 M citric acid aqueous solution with stirring overnight, followed by washing with water 5 times. The resulting dispersion had a pH of 3.9.

The mixture of 30 nm cubic ceria ENMs with nanorods was synthesized using a hydrothermal method [31]. Typically, 0.9 mmol cerium nitrate was dissolved into 15 ml 9 M sodium hydroxide solution with stirring for 0.5 h. The suspension was transferred into

a Teflon-lined stainless steel bomb and heated at 140 °C for 48 h. After the hydrothermal treatment, fresh precipitates were separated by centrifugation, and washed with deionized water three times. The wet precipitates were dispersed into 0.06 M citric acid aqueous solution overnight, washed with water for several times until the final suspension had a pH around 7.

Fifty-five nm ceria ENM was synthesized by a method [32] modified with controlled thermal treatment to achieve the desired ceria particle size (unpublished results). It was re-dispersed in citrate solution and washed three times in doubly distilled water to remove free cerium and citrate. The resulting dispersion had a pH of 7.

Ceria characterization

The morphology, crystallinity, and phase purity of each citrate-coated ceria ENM were determined in our laboratories using high resolution-transmission electron microscopy/scanning transmission electron microscopy and X–ray diffraction analyses. Primary particle size distributions were determined by TEM analysis [33]. The crystallinity of all ceria ENMs were determined by XRD (Siemens 5000 diffractometer). Particle size distributions in aqueous suspension were determined using dynamic light scattering (90Plus Nanoparticle Size Distribution Analyzer, Brookhaven Instruments Corp, Holtsville, NY). To indicate the stability of the ceria dispersion when infused into the rat, the zeta potential was measured for each ENM (except the mixture of ceria nanoparticles and nanorods) using a Zetasizer nano ZS (Malvern Instruments, Worchestershire, UK). The Zetasizer estimates the surface charge of nanoparticles

based on the assumption that the correlations are generated from spheres, but nanorods have an elongated axis and different mobility from spherical nanoparticles; the instrument therefore often fails to provide consistent and accurate estimation for nanorods and mixtures that include rods. Since all of the ceria ENMs had hydrodynamic diameters < 200 nm, the Hückel approximation was used to calculate zeta potential from electrophoretic mobility. To estimate the extent of citrate surface coating each of the ceria ENMs was washed at least three times with water before drying. As separation of the 5 nm ceria by centrifugation required ~12000 rpm for 12 h due to their small size, they were agglomerated by decreasing the pH to 4, enabling centrifugation. Thermogravimetric analysis (Perkin-Elmer TGA7 Analyzer) was then performed to investigate the weight loss of citrate-coated ceria NPs over the temperature range of 150 to 300°C under which decomposition of citric acid occurs. The extent of citrate surface coating was estimated based on the assumption that all the ceria NPs were spherical and had uniform size. The free cerium concentration in the ceria dispersions of the unwashed 5 nm ceria and each of the washed ENMs was determined using Amicon Ultra-4 centrifugal 3000 molecular weight cut-off filter devices and centrifugation at 3000 g to obtain filtrate, which was analyzed for cerium by ICP-MS.

Animals

Data were obtained from 101 male Sprague Dawley rats, weighing 325 ± 30 g (mean ± SD), that were housed individually in the University of Kentucky Division of Laboratory Animal Resources facility. All animal studies were approved by the University of Kentucky Institutional Animal Care and Use Committee. The research was conducted in

accordance with the Society of Toxicology's Guiding Principles in the Use of Animals in Toxicology (http://www.toxicology.org/ai/air/air6.asp).

Cerium ion and ceria ENM administration

Rats were prepared with 2 cannulae, surgically inserted into femoral veins under ketamine/xylazine anesthesia, which terminated in the vena cava, and were connected to infusion pumps via a flow-through swivel. This enabled conduct of the study in the awake, mobile rat. All samples were sonicated to ensure dispersion prior to administration. The day after cannulae implantation the un-anesthetized rat was infused via the longer cannula with cerium ion (as the chloride), a ~ 5% ENM dispersion in water, or water. A pilot study was conducted with the cerium ion and each of the ceria ENMs to determine tolerability following iv infusion. A 100 mg cerium ion/kg infusion was lethal. Rats were infused with ~250 or 175 mg/kg of the 5 nm ceria; 3 of 8 died. A dose of ~250 mg of the 15 nm ceria/kg was tolerated. Infusion of 100 mg/kg of the 30 nm ceria resulted in some evidence of mild distress (tachypnea, skittish behavior, and not resting well). Dyspnea and lethargic were seen in rats given 250, 100 or 78 mg of the 55 nm ceria/kg. Therefore the target doses were 100 mg/kg for the 5, 15, and 30 nm ceria and 50 mg/kg for the 55 nm ceria ENM and the cerium ion. ICP-MS analysis of cerium in replicate samples of the dosed materials showed the doses to be 70 to 100% of the target doses. Each was infused over 1 h, except for the cerium ion that was infused over 2 h. Control rats received water adjusted to the pH of the paired ceria ENM or cerium ion. To compensate for the iv administration of a considerable volume of grossly hypotonic infusion, concurrent iv infusion of an equal volume and rate of 1.8%

sodium chloride in water was delivered into the second, shorter, cannula. Each fluid was delivered at ~ 0.6 ml/h.

Sample collection

After the infusion, 0.6 ml blood was withdrawn at 0.167, 0.5, 0.75, 1, 2 and 4 h from the cannula that had not delivered ceria from 3 rats that had received infusion of the cerium ion, 6 that received the 30 nm ceria ENM, and 5 that received the 5, 15, 55 or 30 nm ceria cube + rod ENM. The blood sample was immediately separated volumetrically into two 0.3 ml aliquots to enable determination of Ce in whole blood in one and in the serum and clot fractions of the other. A blood clot is formed by platelets and blood proteins, including fibrin, and traps the blood's red and white cells. It may have some serum trapped in it; therefore the clot fraction may over-estimate the percentage of Ce associated with cells. To determine the distribution of Ce in the serum and clot fractions the 0.3 ml sample of whole blood was allowed to clot at room temperature, the clot given time to contract, and serum withdrawn into a digestion vessel. The clot was withdrawn and placed in another digestion vessel and the remaining serum added to the serum sample. This enabled determination of the mass amount of Ce in the two major compartments of blood; serum and, from the clot fraction, association with the formed elements (red cells, white cells and platelets). This approach was taken to avoid centrifugation to generate the serum sample because we found that centrifugation at 1600 g for 10 min, as used to generate serum, resulted in loss of ~ 75% of a 30-nm ceria ENM from the serum sample [18].

Blood was also obtained from some rats 20, 168 (1 week) or 720 h (1 month) after ceria ENM administration. An equal volume of saline was infused after each blood withdrawal to replace the fluid volume. Blood was obtained at termination of all rats.

Cerium analysis:

To determine Ce in whole blood the sample was transferred into a 55 ml TFM (polytetrafluoroethylene) digestion vessel (CEM) to which 6 ml trace-metal grade nitric acid and 3 ml 30% H_2O_2 were added, digested in a CEM MARS Xpress microwave at 180 °C for 10 min to convert all ceria to dissolved Ce^{4+}, diluted with 18 MΩ water to 50 ml, and subsequently further diluted dependent on the Ce concentration.

Cerium concentration was determined in whole blood, serum and clot by ICP-MS (Agilent 7500cx, Santa Clara, CA, U.S.). Following ceria ENM administration, Ce concentration is believed to reflect the Ce in ceria ENM because ceria ENMs are quite inert and persist as an ENM in the rat for months [34], and the Ce levels in non-Ce treated rats is very low. We determined a method detection limit (MDL) of Ce for blood and serum samples of 0.018 mg/L [18]. No samples in this study had Ce concentrations below this MDL. Seven samples, containing whole blood, serum or clot, were analyzed in duplicate and were spiked with 8.3 ng Ce/ml. Results of duplicate analysis showed a range of 0 to 4% between the two determinations. Recovery of the Ce spike ranged from 93 to 114%, averaging 105%.

Data analysis and statistics:

Blood, serum and clot Ce concentrations were normalized to an infusion dose of 100 mg ceria/kg for all rats, based on determination of the actual Ce content of the infusions by ICP-MS analysis, and because a few materials were given at doses other than 100 mg/kg, as noted above. This enabled direct comparison of results from the cerium ion, ceria ENM sizes, and shapes. Outliers, identified using the Grubbs test, were not included in the data analysis. Four percent of the 600 whole blood, serum and clot samples were outliers by this test.

Pharmacokinetic modeling. Non-compartmental and compartmental analyses of the whole blood Ce concentration vs. time results were conducted using WinNonLin, a pharmacokinetic analysis program (Pharsight®, St. Louis, Missouri). For non-compartmental analysis, AUC (h*mg/L), C_{max} (mg/L), half life ($t_{1/2}$, h), and mean residence time (MRT, h) were calculated. The squared correlation of distances (Rsq) and correlation between time (X) and Ce concentration (Y) (Corr-XY) were used to measure the goodness of fit. For compartmental analysis, one and two compartments were evaluated to determine the best model fit. AUC (h*mg/L), C_{max} (mg/L), half life ($t_{1/2}$, h), mean residence time (MRT, h), clearance (CL, ml/h/kg) and apparent volume of distribution at steady state (Vd_{ss}) were calculated. Various weightings were evaluated, including 1, 1/y (y: ceria concentration, which weights higher values more heavily), $1/y^2$ (which weights lower values more heavily), 1/predicted concentration (iterative reweighting), and 1/predicted concentration^2. Goodness of fit was based on visual inspection, weighted corrected sum of squares, sum of square residuals, weighted sum of square residuals, random distribution of residuals, Akaike's information criteria, and Swartz criteria. The initial estimates for model parameters were calculated as below.

The semi-logarithmic plots of blood concentration vs. time data showed the one or two compartment kinetics model as $C(t) = Re^{-\lambda t}$ and $C(t) = R_1e^{-\lambda 1t} + R_2e^{-\lambda 2t}$, respectively. R_1 and R_2 represent intercepts on the concentration (Y) axis of the back-extrapolated initial and terminal phases and λ_1 and λ_2 = the initial and terminal slopes. As blood sampling began after completion of the infusion, the iv bolus case was used. $A = \frac{D_{iv}\lambda}{k_o(1-e^{-\lambda t})} R$ was used to correct the infusion intercept values for the one compartmental analysis and $A_1 = \frac{D_{iv}\lambda_1}{k_o(1-e^{-\lambda 1t})} R_1$ and $A_2 = \frac{D_{iv}\lambda_2}{k_o(1-e^{-\lambda 2t})} R_2$ were used in the two compartment model. D_{iv} is the infusion dose, k_o is the infusion rate. $V_1 = \frac{D_{iv}}{A1+A2}$ was used to calculate the volume of the central compartment. The micro rate constants were determined as $k_{21} = \frac{\lambda_2 \times A_1 + \lambda_1 \times A_2}{A_1 + A_2}$; $k_{10} = \frac{\lambda_2 \times \lambda_1}{K_{21}}$; and $k_{12} = \lambda_1 + \lambda_2 - k_{10} - k_{21}$. k_{12} and k_{21} represent the rate constants between central and peripheral compartment, and k_{10} is the elimination rate constant from the central compartment. The elimination half-lives ($t_{1/2}$) were calculated as $t_{1/2\lambda 1} = 0.693/\lambda_1$ and $t_{1/2\lambda 2} = 0.693/\lambda_2$. One-way ANOVA, followed by Tukey's multiple comparison tests (Prism 5.02 software, GraphPad, San Diego, CA), was used to test for significant differences in pharmacokinetic parameters among the 6 treatment groups.

Quality analysis of the WinNonLin coefficients was conducted by determining whether the ratio of the coefficient estimate to its average standard error was greater than the appropriate p value < 0.05, using a two-tailed Student's t-test (3.18 for n = 3, 2.78 for n = 4), Excel and Systat. The results showed that the pharmacokinetic parameter estimations using WinNonLin were acceptable for only the cerium ion and the 5-nm

ceria ENM. Two factors contributing to this were 1) that less than 2% of the dose of the other 4 ENMs was circulating in the blood when the first sample to estimate the pharmacokinetic parameters was obtained (0.167 h after completion of the infusion), and 2) the Ce concentration increased in blood from 0.167 to 4 h after infusion of the 15- and 30-nm ceria, which is not the elimination behavior for typical pharmacokinetic models. Therefore, the pharmacokinetic data for ceria ENMs was compared directly to that of the cerium ion, which is known to follow typical pharmacokinetic elimination models.

Ratio of Ce concentration in whole blood following infusion of ceria ENMs vs. the cerium ion. The Ce ratio in ceria ENMs compared to the cerium ion was reported as

$$R = \frac{[Ce]_{ceria}}{[Ce]_{cerium(ion)}}$$

$R = R^0 \cdot \exp(-\alpha \cdot t)$ met the t-test criterion, then the trend was described by an apparent first order process.

Ce partitioning between serum and clot. The quality of the data describing the partitioning of Ce between the serum and clot fractions was screened using mass balances. The total mass of cerium (or ceria) in the whole blood sample should equal the sum of the cerium masses in the serum and clot phases. The cut-off for mass material balance screening was taken to be ± 30%. If the sum of the masses of Ce in the serum and clot phases was < 70 or > 130% of that in the mass in the whole blood sample, the partitioning data were not used in the analysis or shown in the figure. No other screening analyses, such as outlier evaluation, were applied. The partitioning of cerium was reported as the ratio of cerium in the serum phase to that in whole blood.

Results:

Particle morphologies are shown in Figure 1. Panel D in Figure 1 is part of a larger image that shows the diameter and length of the rods in the mixture of 30-nm cubic and rod ENMs were ~ 10 nm and 2 μm, respectively. The shape, surface area, zeta potential in water, and estimated extent of the ENM surface that was coated with citrate are shown in Table 1. All of the ceria ENMs had face-centered cubic (FCC) crystal structures with the same Miller indices of (111), (220) and (311), and with lesser presence of (200), (222) and (400), based on XRD crystal structure linked to known morphology. The 55 nm ceria had the lowest surface coating of citrate and a lower absolute surface charge (-31.5mV) than the other ENMs. The unwashed 5 nm ceria ENM had 11.6 ± 0.3% free cerium in the dispersion. The washed ceria ENMs were found to contain << 1% free cerium.

Ten min (0.167 h) after completion of the cerium ion or 5-nm ceria ENM infusion ~ 14 and 32% of the Ce remained in the circulating blood, respectively. This was calculated from the measured blood Ce concentration compared to the Ce dose, based on the iv infusion of 100 mg ceria/kg into the rat's vascular system (~ 7% of its body volume), which would introduce ~ 1163 mg Ce/l blood. In contrast, the 15-, 30- and 55-nm ceria and mixture of 30-nm cubic + rod ceria were rapidly removed from circulation, so that 0.167 h after their infusion ≤ 2% was in blood (Figure 2).

Pharmacokinetic models were constructed using whole blood Ce concentrations from each individual rat's results. Non-compartmental models showed the best fits for the cerium ion (Rsq 0.94 ± 0.08, Corr XY = 0.97 ± 0.04) and 5 nm ceria ENM (Rsq 0.89 ±

0.06, Corr XY = 0.94 ± 0.03). However, 15, 30 cubic, 30 cubic + rods, and 55 nm ceria ENMs were poorly fitted by non-compartmental modelss. One and two compartment models showed the Ce concentrations in blood obtained 0.167 h to 1 week after cerium ion infusion and 0.167 h to 30 day following infusion of 5-, 15-, and 30- nm ceria ENMs were best fit by two compartmental models (biexponential decay). For the mixture of 30-nm cubic + rod ceria and the 55-nm ceria ENMs, for which modeling was based on results to 4 h after their infusion, the one compartment model provided the best fit.

Table 2 summarizes the pharmacokinetic parameters. Compartmental analysis showed the cerium ion to have a greater AUC than the ceria ENMs, a higher C_{max} compared to the ≥ 15 nm ENMs, and a smaller Vd_{ss} than all of the ENMs. Surprisingly, the 15- and 30-nm cubic ceria materials showed increasing blood concentrations over the period 0 to 4 h after infusion, with estimated half-lives of this process of ~ 4 and 2.7 h, respectively (Figure 2). Since conventional elimination models are always monotonically decreasing in solute concentration, the WinNonLin fits were poor and the 15 and 30 nm ceria ENMs model coefficients did not meet the Student's t-test criteria for quality (the average standard error was often larger than the estimated value of the coefficient). With the exception of the 5-nm ceria ENM, the pharmacokinetic results are based on < 2% of ceria dose that was remaining in the blood 0.167 h after completion of the ceria infusion, therefore the pharmacokinetic parameter estimates describe only a small fraction of the dose of these ENMs. The two-compartment models for each of the rats that received cerium ion or 5-nm ceria ENM infusions fit the data very well based on visual inspection, weighted corrected sum of squares, sum of square residuals,

weighted sum of square residuals, random distribution of residuals, Akaike's information criteria, and Swartz criteria.

Figure 3 shows the ratio of the whole blood Ce concentration after infusion of 5-, 15-, 30-, and 55-nm ceria ENMs vs. the cerium ion. The ratio, R, for 5 nm ceria ENM could be modeled either by a power law dependence, $R = R_0 \cdot t^d$ (R_0 is a constant and d is the power exponent for time *t*), or an exponential dependence, $R = R_0 \cdot \exp(d \cdot t)$ (R_0 is the Arrhenius-type factor and d is the process rate constant) for each of three animals. Trend lines are shown for the power law dependence (Figure 3, top panel) with d ~ -0.8. Five-nm ceria ENMs are fitted by two-compartment models and their concentrations have apparent links to those of cerium ions, but with different time dependencies. Over the time period, 0 to 4 h after infusion, it was cleared faster than the free ion. On the other hand, R values for both 15 and 30 nm ceria increased over the 0 to 4 h time period and their exponential coefficients were similar (d = 0.41 h^{-1} and d = 0.45 h^{-1}, respectively). The R value of 55 nm ceria showed no strong trend.

The Ce mass balance for cerium ion, calculated by comparing the cerium in the serum plus clot samples to the cerium in whole blood, averaged 98 ± 7% over all samples. For the 5-nm ceria ENM, the average mass balance was 83 ± 44%; 5 out of the total of 30 values from the 6 sample times were below the cutoff of 70% mass balance. These ranged from 16 to 31% and were obtained 120 or 240 min after the ceria infusion, at a time when Ce concentrations had decreased to an average of 8 and 0.4 microgram Ce in the serum prepared from the 0.3 ml of blood. They were not used in the data

analysis. For the remaining 25 values, recovery was 93 ± 40%. For the 15-, 30-, and 55-nm ceria ENMs, 17, 16 and 11 of the 18 values from 3 of the rats met the material balance quality control criteria and were used in the data analysis, respectively. For the 30-nm ceria cubes and rods mixture, 12 values from 2 rats met the material balance quality control criteria and were used in the data analysis.

Figure 4 shows the ratio of Ce distribution in blood serum vs. whole blood from 0.167 to 4 h after completion of the cerium ion or ceria ENM infusions. The complement to this is the ratio of Ce in the clot (associated with the red and white cells and platelets) vs. whole blood fraction (not shown). The ratio of Ce in serum vs. whole blood shows its distribution between blood serum and (the clot fraction). Blood samples taken from 0 to 4 h after infusion showed that the cerium ion, 5-, and 55-nm ceria ENMs did not preferentially distribute into either the blood serum or clot (containing red, white cells and platelets); there was no consistent time dependence of the ratio for all animals. The 30 nm cubic + rod mixture preferentially distributed to the clot fraction over a similar period, also with no consistent time dependence of the ratio for all animals. However, serum/clot partition data for 15- and 30-nm ceria showed that these ENMs migrated into the clot fraction, and that partition ratio ceria in the clot increased with time. Two of the rats that received 15 nm and 4 that received 30 nm ceria showed a statistically significant increase of Ce associated with the clot fraction.

Discussion:

The crystal structure of the ceria ENMs was as expected because the fluorite structure is the only one for crystalline CeO_2. The citrate coating was least dense on the 55 nm ceria, suggesting it would be the most likely of the ENMs test to agglomerate in aqueous dispersion; a problem that was observed during its administration requiring frequent agitation of the dispersion to prevent it from occluding the infusion line. Although nearly 12% of the total cerium in the 5 nm ceria ENM was free cerium in the aqueous phase, comparison of the results after infusion of the 5 nm ceria ENM, the cerium ion, and the other ceria ENMs shows the free cerium cannot account for the differences between the 5 nm and the larger ENMs.

In the present study ~ 14% of the cerium ion remained in the blood 0.167 h after completion of a 1 h iv infusion. In a previous report Ce was determined in blood from 1 h to 3 days following its iv administration as the chloride to mice and rats; however, the author did not conduct a pharmacokinetic analysis of the results [35]. Using WinNonLin to conduct pharmacokinetic analysis, non-compartmental and compartmental calculations of the Bjondahl results [35] showed similar AUC, MRT, C_{max}, and CL results. The non-compartmental half-life (10 h) was the same as the terminal half-life obtained with a two compartment model, which best fit the data for compartmental analysis. The initial half-life of the Bjondahl results (~ 3 h) was longer than we obtained (0.6 h) because our study included samples taken as early as 10 min, whereas the first sample in the Bjondahl study was obtained at 1 h.

Ten min after completion of the iv infusion of ceria ENMs, ~ 32% of the 5-nm ceria but < 2% of the larger ceria ENMs were present in the blood. The greater extent of citrate coating on the 5-nm ceria (and therefore its greater hydrophilicity) may have contributed to this. However, we do not know how long the citrate persisted on the surface of the ceria ENM or if was covered (opsonized) by proteins. The rapid clearance of metal/metal oxide ENMs from blood has been reported previously.

Little has been reported about the fate of systemic cerium, other than it is very slowly eliminated, primarily in bile, resulting in prolonged retention in mammals, primarily in the liver and skeletal system [36, 37]. Our pharmacokinetic results showed that the cerium ion had a smaller Vd_{ss} than the 5-nm ceria ENM. It also showed less retention in reticuloendothelial tissues, but more in the lung [34]. All the ceria ENMs showed a large Vd_{ss} indicating great distribution in tissues, consistent with the intracellular agglomerations we have seen, especially in reticuloendothelial cells. Ceria ENMs have been seen in the cytoplasm of brain cells, phagosomes of macrophages, vesicles of lung fibroblasts, spleen red pulp, Kupffer cells, hepatocytes and mesangial cells [18, 20, 38-41]. Thirty days after ceria ENM infusion the greatest concentration was seen in the reticuloendothelial tissues, including liver and spleen [18, 20, 42]. It was reported that lung, heart, and brain cerium did not decrease over 6 months following iv ceria ENM dosing [39]. A study with the 30-nm ceria ENM used in the present study showed no significant decrease of ceria in 14 tissues up to three months after iv administration. The highest concentrations were in reticuloendothelial tissues (spleen, liver and bone marrow), followed by the lung, then other sites [34]. We are not aware of any reports of

ceria uptake into red or white blood cells or platelets other than our prior finding suggesting a small amount of a 30 nm ceria ENM might have entered red blood cells after 1 h *in vitro* [18]. It is unclear if the ceria ENMs would ever reach a constant blood level. Up to the times studied in the present report, there was generally a decrease of blood cerium. Given the persistence of ceria in the rat, one might expect a steady state to be reached. However, 90 days after ceria infusion blood cerium concentration was higher than earlier times [34].

The cerium ion was equally distributed between serum and clot fractions. A previous study reported that 2 h after iv cerium ion administration ~ 28% of the cerium in the blood was in cells and 72% in serum [43], similar to results in the present study that showed ~ 70% in the serum fraction at 2 h. The distribution of ceria ENMs between serum and clot varied with size and surface chemistry. The 5-nm ceria was evenly distributed within the serum and clot fractions. We previously observed small agglomerations of the 5-nm ceria in serum, presumably associated with proteins, and agglomerations associated with the extracellular side of the erythrocyte cell membrane after 1 h of incubation of the ceria in blood [20]. The ability of ENMs to enter erythrocytes, a non-phagocytic cell, has been observed for 78 nm polystyrene, 25-nm gold, and 22-, 25- and 80-nm titania ENMs [44-46]. However, we are not aware of any studies of ceria ENM or other metal/metal oxide ENMs entry into white blood cells or platelets.

Although the extent of citrate coating might be expected to influence the fate of ceria ENMs *in vivo*, the present results show no clear trends between the extent of citrate surface coating and ceria ENM distribution between serum and the clot fraction initially, or over time. For the cerium ion, and 5- and 55-nm and the mixture of 30-nm cubic + rod ceria ENMs, we were unable to identify any trends in the percentage of Ce in the serum vs. time.

The blood levels of the 15- and 30-nm ceria ENMs increased over the 4 h after their infusion. As they were given by the iv route, this suggests a re-distribution of the ENM over time. Redistribution of ENMs has been previously recognized and discussed, e.g. [47]. An increase of ENM in blood within the first 2 h after iv administration has been reported, although the increases appear to be within the variability of the reported measure of the quantum dots in plasma or blood and neither report discusses the increase [48, 49]. The increase we saw may be influenced by opsonization and/or distribution into and out of a non-central compartment, such as the lymphatic system, as noted by [50]. We also observed that the distribution of the 15- and 30-nm ceria ENMs within blood compartments changed over the 4 h after completion of their infusion, when they became more associated with the cells in the clot fraction. These results suggest their surface chemistry changed during that period, which may be due to dissociation of the citrate, association with proteins or blood cells, and/or cell entry and release. Nanoscale materials are rapidly coated with plasma proteins and other circulating substances, which create a corona around the ENM, increasing their hydrodynamic size [51, 52]. It has been shown that citrate-coated ENMs bind to the surface of cells [24]

and can become opsonized with albumin [27]. We speculate that the increase of the 15- and 30-nm ceria ENMs in circulating blood and migration toward the clot fraction during the first 4 h after their iv infusion is due to distribution out of, then back into, circulating blood, perhaps associated with opsonization. This might be due to initial accumulation in blood vessels or adsorption onto the luminal surface of vascular endothelial cells, followed by opsonization and re-circulation in blood. However, we would not anticipate extensive accumulations of ceria blocking the vasculature in the absence of cardio- and cerebrovascular incident (MI and stroke) which we have not observed in these rats that generally tolerated the target doses well. Or the ceria ENMs may have distributed outside of the vascular compartment, such as entrapment by reticuloendothelial organs followed by their release them back into blood, or entry into the lymphatic system, that drains into the cardiovascular system. Particles up to 50 nm are able to rapidly enter the lymphatic system [53, 54]. From the results of the present study we do not have evidence of the origin of the ceria ENMs that re-entered circulating blood during the first 4 h after their infusion. However, we have seen a net migration of Ce following 30-nm ceria ENM administration from liver to spleen from 1 to 20 h after its infusion [55] and into lung over 90 days, consistent with re-distribution of this ENM over time [34]. As > 98% of the ceria dose was no longer in circulating blood when we started blood sampling 10 min after completion of the ceria infusion, the long terminal half-life and MRT and large Vd_{ss} for the 5, 15 and 30 nm ceria ENMs, based on blood levels to 30 days, may describe the very small fraction of the ENMs that had not yet distributed out of blood and/or ceria re-distributing among storage sites. This speculation is based on the retention of very large percentage of the ceria ENM dose for

a long time in the rat and evidence we (and others) have of re-distribution among sites over time. Similarly, there may have been some re-distribution of the 5 nm ceria which was not seen above the much higher level of ceria remaining in blood from the infusion during the first 4 h after its infusion.

The non-compartmental analysis could not estimate some of the pharmacokinetic parameters for the 15 and 30 nm ceria ENMs probably because of the ceria concentration increase at the first 4 h. Due to the lack of prior studies of metal and metal oxide ENMs in blood, further studies of citrate-coated ceria ENMs are necessary to better understand their fate in the vascular compartment, including the stability of the citrate coating; their interaction with cell membranes; and the rate, extent and character of protein association.

The mean residence time (MRT) typically indicates the average time molecules stay in the body. In our study, the MRT indicated how long ceria ENMs remained in blood, not in the tissues, because MRT is derived from measurement of ceria (as Ce) in blood [56]. It has been previously noted that the blood half-life of an ENM may be short despite prolonged body persistence, due to reticuloendothelial system entrapment and other processes not typical of small inorganic and organic molecules [19]. Non-compartmental and compartmental analyses produced quite different MRT results, although the trends among the tested materials are similar across analysis. The lower MRT values with the non-compartmental analysis may be due to its tendency to underestimate MRT [57].

Knowing that there are persistent accumulations of ceria ENMs in multiple organs suggests the MRT results from the compartmental analysis more closely reflects the whole body residence time of ceria ENMs. The results of the present pharmacokinetic calculations that one can have the most confidence in are those obtained following infusion of the cerium ion and the 5-nm ceria ENM, due to the very rapid clearance of the larger ENMs from circulating blood and the rise in Ce concentration over 4 h following 15- and 30-nm ceria ENM infusion. Although the results obtained with the cerium ion and 5, 15 and 30 nm ceria ENMs clearly show two compartments, the values for the second compartment do not have a high degree of precision due to the limited number of data points on which they are based.

It has been previously noted that some of the properties of ENMs, e.g., opsonization, adhesion, and phagocytic uptake, may differ from small organic molecule disposition for which pharmacokinetic modeling programs such as WinNonLin were created [19]. Pharmacokinetic and PBPK approaches have been used to model ENM distribution among tissues and blood [58, 59]. Most nanomaterials do not exhibit ADME profiles typical of drugs [60], e.g. they are rapidly cleared from the blood, not metabolized, and not rapidly eliminated, unless small enough to be filtered by the renal glomerulus. It has been recognized that the toxicokinetics of ENMs are unlikely to follow the “rules” of current approaches [61, 62]. Further work is needed to develop a pharmacokinetic model to predict the time-dependent changes of ceria ENM distribution in tissues and blood.

There is considerable literature on the pharmacokinetics of polymer ENMs due to the extensive research in developing them as drug delivery systems. Much less is known about the pharmacokinetics of metal and metal oxide ENMs; particularly their distribution, residence time, and rate of clearance from the vascular compartment. The present study informs about the effects of ENM physicochemical properties on distribution and clearance from blood. The results show ceria ENMs have a biodistribution and clearance pattern which cannot be predicted from the cerium ion. This may be due to the very different physicochemical properties of the cerium ion and ceria ENMs.

Conclusions:

To better understand the fate of ceria as a model ENM we compared the distribution within, and rate of clearance from, blood of four different sizes of cubic or polyhedral ceria nanoparticles, a mixture of cubes and rods, and the cerium ion after iv infusion into rats. Table 3 summarizes the main findings of the present study. The kinetics and distribution of the cerium ion did not predict those of the ceria ENMs. A 5-nm ceria ENM, which was very resistant to agglomeration and settling *in vitro,* was cleared much more slowly from blood than larger ceria ENMs, presumably because it was too large to be cleared by glomerular filtration and perhaps too small or too hydrophilic to be readily recognized by the reticuloendothelial system. Ceria ENMs larger than 5 nm were very rapidly cleared from circulating blood. All the ceria ENMs had a much greater Vd_{ss} than the cerium ion, consistent with their extensive distribution and prolonged retention throughout the rat. The 15 and 30 nm ceria ENMs showed concentration ratios increasing vs. cerium ion over 4 h after infusion. The distribution of ceria ENMs

between serum and the blood clot was size dependent. The citrate-coated 30-nm ceria showed the greatest distribution in the clot fraction. The fraction of 15 and 30 nm-ceria ENMs in the clot fraction increased over 4 h, suggesting a change in their surface properties, perhaps due to opsonization. A further understanding of the rate and nature of ceria ENM association with blood proteins and cells, and the process(es) of their clearance from blood, is needed to fully interpret their fate in the vascular compartment.

References

1. Batrakova EV, Kabanov AV: Pluronic block copolymers: evolution of drug delivery concept from inert nanocarriers to biological response modifiers. *J Control Release* 130(2), 98-106 (2008).
2. Kanwar Jr, Mahidhara G, Kanwar RK: Recent advances in nanoneurology for drug delivery to the brain. *Current Nanosci* 5(4), 441-448 (2009).
3. Karakoti AS, Monteiro-Riviere NA, Aggarwal R *et al.*: Nanoceria as antioxidant: synthesis and biomedical applications. *JOM* 60(3), 33-37 (2008).
4. Tarnuzzer RW, Colon J, Patil S, Seal S: Vacancy engineered ceria nanostructures for protection from radiation-induced cellular damage. *Nano Lett* 5(12), 2573-2577 (2005).
5. Niu J, Azfer A, Rogers Lm, Wang X, Kolattukudy PE: Cardioprotective effects of cerium oxide nanoparticles in a transgenic murine model of cardiomyopathy. *Cardiovasc Res* 73(3), 549-559 (2007).
6. Xia T, Kovochich M, Liong M *et al.*: Comparison of the mechanism of toxicity of zinc oxide and cerium oxide nanoparticles based on dissolution and oxidative stress properties. *ACS Nano* 2(10), 2121-2134 (2008).
7. Schubert D, Dargusch R, Raitano J, Chan SW: Cerium and yttrium oxide nanoparticles are neuroprotective. *Biochem Biophys Res Comm* 342(1), 86-91 (2006).
8. Singh N, Cohen CA, Rzigalinski BA: Treatment of neurodegenerative disorders with radical nanomedicine. *Ann N Y Acad Sci* 1122, 219-230 (2007).

9. D'angelo B, Santucci S, Benedetti E *et al.*: Cerium oxide nanoparticles trigger neuronal survival in a human Alzheimer disease model by modulating BDNF pathway *Current Nanosci* 5(2), 167-176 (2009).

10. Chen J, Patil S, Seal S, Mcginnis JF: Rare earth nanoparticles prevent retinal degeneration induced by intracellular peroxides. *Nat Nanotechnol* 1(2), 142-150 (2006).

11. Das M, Patil S, Bhargava N *et al.*: Auto-catalytic ceria nanoparticles offer neuroprotection to adult rat spinal cord neurons. *Biomaterials* 28(10), 1918-1925 (2007).

12. Park EJ, Choi J, Park YK, Park K: Oxidative stress induced by cerium oxide nanoparticles in cultured BEAS-2B cells. *Toxicology* 245(1-2), 90-100 (2008).

13. Thill A, Zeyons O, Spalla O *et al.*: Cytotoxicity of CeO_2 nanoparticles for *Escherichia coli.* Physico-chemical insight of the cytotoxicity mechanism. *Environ Sci Technol* 40(19), 6151-6156 (2006).

14. Brunner TJ, Wick P, Manser P *et al.*: *In vitro* cytotoxicity of oxide nanoparticles: comparison to asbestos, silica, and the effect of particle solubility. *Environ Sci Technol* 40(14), 4374-4381 (2006).

15. Eom HJ, Choi J: Oxidative stress of CeO_2 nanoparticles *via* p38-Nrf-2 signaling pathway in human bronchial epithelial cell, Beas-2B. *Toxicol Lett* 187(2), 77-83 (2009).

16. Lin W, Huang YW, Zhou XD, Ma Y: Toxicity of cerium oxide nanoparticles in human lung cancer cells. *Int J Toxicol* 25(6), 451-457 (2006).

17. Park E-JC, Wan-Seob, Jeong J, Yi J-H, Choi K, Kim Y, Park K: Induction of inflammatory responses in mice treated with cerium oxide nanoparticles by intratracheal instillation. *J Health Sci* 56(4), 387-396 (2010).

18. Yokel RA, Florence RL, Unrine JM *et al.*: Biodistribution and oxidative stress effects of a systemically-introduced commercial ceria engineered nanomaterial. *Nanotoxicology* 3(4), 234-248 (2009).

19. Riviere JE: Pharmacokinetics of nanomaterials: an overview of carbon nanotubes, fullerenes and quantum dots. *Wiley Interdiscip Rev Nanomed Nanobiotechnol* 1(1), 26-34 (2009).

20. Hardas SS, Butterfield DA, Sultana R *et al.*: Brain distribution and toxicological evaluation of a systemically delivered engineered nanoscale ceria. *Toxicol Sci* 116(2), 562-576 (2010).

21. Riddick TM: *Control of colloidal stability through zeta potential*. Livingston Publishing Co., Wynnewood, PA, pp 320-331 (1968).

22. Gaur U, Sahoo SK, De TK, Ghosh PC, Maitra A, Ghosh PK: Biodistribution of fluoresceinated dextran using novel nanoparticles evading reticuloendothelial system. *Int J Pharm* 202(1-2), 1-10 (2000).

23. Niidome T, Yamagata M, Okamoto Y *et al.*: PEG-modified gold nanorods with a stealth character for in vivo applications. *J Control Release* 114(3), 343-347 (2006).

24. Cao T, Yang T, Gao Y, Yang Y, Hu H, Li F: Water-soluble NaYF4:Yb/Er upconversion nanophosphors: Synthesis, characteristics and application in bioimaging. *Inorg Chem Commun* 13(3), 392-394 (2010).

25. Frasca G, Gazeau F, Wilhelm C: Formation of a three-dimensional multicellular assembly using magnetic patterning. *Langmuir* 25(4), 2348-2354 (2009).

26. Pallem VL, Stretz HA, Wells MJ: Evaluating aggregation of gold nanoparticles and humic substances using fluorescence spectroscopy. *Environ Sci Technol* 43(19), 7531-7535 (2009).

27. Brewer SH, Glomm WR, Johnson MC, Knag MK, Franzen S: Probing BSA binding to citrate-coated gold nanoparticles and surfaces. *Langmuir* 21(20), 9303-9307 (2005).

28. Masui T, Hirai H, Imanaka N, Adachi G, Sakata T, Mori H: Synthesis of cerium oxide nanoparticles by hydrothermal crystallization with citric acid. *J Mat Sci Lett* 21(6), 489-491 (2002).

29. Pan C, Zhang D, Shi L: CTAB assisted hydrothermal synthesis, controlled conversion and CO oxidation properties of CeO2 nanoplates, nanotubes, and nanorods. *J Solid State Chem* 181(6), 1298-1306 (2008).

30. Mai H-X, Sun L-D, Zhang Y-W *et al.*: Shape-selective synthesis and oxygen storage behavior of ceria nanopolyhedra, nanorods, and nanocubes. *J Phys Chem B* 109(51), 24380-24385 (2005).

31. Wu Q, Zhang F, Xiao P *et al.*: Great influence of anions for controllable synthesis of CeO_2 nanostructures: From nanorods to nanocubes. *J Phys Chem C* 112(44), 17076-17080 (2008).

32. Zhang F, Jin Q, Chan S-W: Ceria nanoparticles: Size, size distribution, and shape. *J Appl Phys* 95(8), 4319-4326 (2004).

33. Mandzy N, Grulke E, Druffel T: Breakage of TiO2 agglomerates in electrostatically stabilized aqueous dispersions. *Powder Technol* 160(2), 121-126 (2005).

34. Yokel RA, Au TC, MacPhail R *et al.*: Distribution, elimination and biopersistence to 90 days of a systemically-introduced 30 nm ceria engineered nanomaterial in rats. *Nanotoxicology*, (in preparation).

35. Bjondahl K: Differences in liver weight, mortality in cerium-treated mice and 144Ce levels in blood, liver, urine and faeces at various intervals after treatment with nafenopin and pregnenolone 16-alpha-carbonitrile (PCN). *Medical Biol* 54(6), 454-460 (1976).

36. Moskalev YI: [Experiments on distribution of Ce 144]. *Med Radiol (Mosk)* 4(5), 52-58 (1959).

37. Takada K, Fujita M: Effects of DTPA on the excretion and tissue distribution of 144Ce administered subcutaneously, intramuscularly and intravenously in rats. *J Radiat Res (Tokyo)* 14(2), 187-197 (1973).

38. Limbach LK, Li Y, Grass RN *et al.*: Oxide nanoparticle uptake in human lung fibroblasts: effects of particle size, agglomeration, and diffusion at low concentrations. *Environ Sci Technol* 39(23), 9370-9376 (2005).

39. Rzigalinski BA, Danelison I, Strawn ET, Cohen CA, Liang C: *Nanoparticles for cell engineering - A radical concept*. In: *Nanotechnologies for the Life Sciences*, Kumar Cssr (Eds). Wiley-VCH, Hoboken, New Jersey 361-387 (2006).

40. Rzigalinski BA, Meehan K, Davis RM, Xu Y, Miles WC, Cohen CA: Radical nanomedicine. *Nanomedicine (Lond)* 1(4), 399-412 (2006).

41. Hirst SM, Karakoti AS, Tyler RD, Sriranganathan N, Seal S, Reilly CM: Anti-inflammatory properties of cerium oxide nanoparticles. *Small* 5(24), 2848-2856 (2009).

42. He XA, Zhang HF, Ma YH *et al.*: Lung deposition and extrapulmonary translocation of nano-ceria after intratracheal instillation. *Nanotechnology* 21(28), (2010).

43. Nakamura Y, Tsumura Y, Tonogai Y, Shibata T, Ito Y: Differences in behavior among the chlorides of seven rare earth elements administered intravenously to rats. *Fundam Appl Toxicol* 37(2), 106-116 (1997).

44. Geiser M, Rothen-Rutishauser B, Kapp N *et al.*: Ultrafine particles cross cellular membranes by nonphagocytic mechanisms in lungs and in cultured cells. *Environ Health Perspect* 113(11), 1555-1560 (2005).

45. Rothen-Rutishauser BM, Schurch S, Haenni B, Kapp N, Gehr P: Interaction of fine particles and nanoparticles with red blood cells visualized with advanced microscopic techniques. *Environ Sci Technol* 40(14), 4353-4359 (2006).

46. Wang J, Zhou G, Chen C *et al.*: Acute toxicity and biodistribution of different sized titanium dioxide particles in mice after oral administration. *Toxicol Lett* 168(2), 176-185 (2007).

47. Yang RS, Chang LW, Wu JP *et al.*: Persistent tissue kinetics and redistribution of nanoparticles, quantum dot 705, in mice: ICP-MS quantitative assessment. *Environ Health Perspect* 115(9), 1339-1343 (2007).

48. Al-Jamal WT, Al-Jamal KT, Cakebread A, Halket JM, Kostarelos K: Blood circulation and tissue biodistribution of lipid--quantum dot (L-QD) hybrid vesicles intravenously administered in mice. *Bioconjug Chem* 20(9), 1696-1702 (2009).

49. Fischer HC, Liu L, Pang KS, Chan WCW: Pharmacokinetics of nanoscale quantum dots: in vivo distribution, sequestration, and clearance in the rat *Advanced Functional Materials* 16(10), 1299-1305 (2006).

50. Li M, Al-Jamal KT, Kostarelos K, Reineke J: Physiologically based pharmacokinetic modeling of nanoparticles. *ACS Nano* 4(11), 6303-6317 (2010).

51. Owens DE, Peppas NA: Opsonization, biodistribution, and pharmacokinetics of polymeric nanoparticles. *Int J Pharm* 307(1), 93-102 (2006).

52. Deng ZJ, Mortimer G, Schiller T, Musumeci A, Martin D, Minchin RF: Differential plasma protein binding to metal oxide nanoparticles. *Nanotechnology* 20(45), 455101/455101-455101/455109 (2009).

53. Uren RF, Hoefnagel CA: *Lymphoscintigraphy*. In: *Textbook of melanoma*, Thompson JF, Morton DL, Kroon BBR (Eds). Martin Dunitz, New York 339-364 (2004).

54. Kim S, Lim YT, Soltesz EG *et al.*: Near-infrared fluorescent type II quantum dots for sentinel lymph node mapping. *Nat Biotechnol* 22(1), 93-97 (2004).

55. Yokel RA, Tseng MT, Dan M *et al.*: Distribution and biopersistence of ceria engineered nanomaterial in rats - influence of size. *Toxicology*, (in preparation).

56. Rowland M, Tozer TN: Clinical pharmacokinetics and pharmacodynamics: Concepts and applications, 4th Ed. Wolters Kluwer, Philadelphia, (2011).

57. Distefano JJ: Noncompartmental vs. compartmental analysis: some bases for choice. *Am J Physiol* 243(1), R1-6 (1982).

58. Yang RS, Chang LW, Yang CS, Lin P: Pharmacokinetics and physiologically-based pharmacokinetic modeling of nanoparticles. *J Nanosci Nanotechnol* 10(12), 8482-8490 (2010).

59. Li M, Al-Jamal KT, Kostarelos K, Reineke J: Physiologically based pharmacokinetic modeling of nanoparticles. *ACS Nano* 4(11), 6303-6317 (2010).

60. Li SD, Huang L: Pharmacokinetics and biodistribution of nanoparticles. *Mol Pharm* 5(4), 496-504 (2008).

61. Nyland JF, Silbergeld EK: A nanobiological approach to nanotoxicology. *Hum Exp Toxicol* 28(6-7), 393-400 (2009).

62. Lee HA, Leavens TL, Mason SE, Monteiro-Riviere NA, Riviere JE: Comparison of quantum dot biodistribution with a blood-flow-limited physiologically based pharmacokinetic model. *Nano Lett* 9(2), 794-799 (2009).

101. Health Effects Institute: Evaluation of human health risk from cerium added to diesel fuel, Communication 9, Boston, MA, http://pubs.healtheffects.org/getfile.php?u=295.

102. Integrated Laboratory Systems, Inc.: Chemical information profile for ceric oxide [CAS No. 1306-38-3]. Supporting Nomination for Toxicological Evaluation by the National Toxicology Program, 21pp, http://ntp.niehs.nih.gov/index.cfm?objectid=0847DDA0-F261-59BF-FAA04EB1EC032B61.

103. Environment Directorate, Joint Meeting of the Chemicals Committee and the Working Party on Chemicals, Pesticides and Biotechnology, Organisation for Economic Co-operation and Development: List of manufactured nanomaterials and list of endpoints for phase one of the sponsorship programme for the testing of manufactured nanomaterials: revision, Series on the safety of manufactured nanomaterials, Number 27, ENV/JM/MONO(2010)46, http://www.oecd.org/officialdocuments/displaydocumentpdf/?cote=env/jm/mono(2010)46&doclanguage=en.

** = of considerable interest [19] Riviere. This is a review of carbon-based and quantum dot ENM pharmacokinetics.

Financial disclosure and conflict of interest declaration:

None of the authors has a financial conflict of interest related to this research. No writing assistance was obtained in the preparation of this report.

Funding: This work was supported by the United States Environmental Protection Agency Science to Achieve Results [Grant Number RD-833772].

Acknowledgements: The authors gratefully acknowledge Rebecca L. Florence for her excellent conduct of aspects of this work and Dr. Robert C. MacPhail for his critical and constructive review of a draft of this report.

Figure legends.

Figure 1. HRTEM and STEM images of ceria used in this study: (a) TEM/STEM: 5-nm polyhedral ceria; (b) TEM: 15-nm polyhedral ceria; (c) TEM: 30-nm cubic ceria; (d) TEM: 30-nm cubic and rod ceria; (e) STEM: 55-nm polyhedral ceria.

Figure 2. Whole blood Ce concentration after completion of iv infusion of the cerium ion, 5, 15, and 30 ceria ENM, a mixture of 30-nm ceria cubes and rods, and 55-nm ceria ENM. All values are normalized to an equivalent dose of 100 mg ceria/kg. Results are mean ± S.D. from 5 rats at each time point, except for cerium ion, where n = 3 for 5 nm ceria ENM where n = 9, 10, 21, 10, 12, and 7 rats at 0.167, 0.5, 1, 2, 20 and 720 h; for 15 nm ceria ENM where n = 10 rats at 0.167, 0.5, 1, 2, and 4 h; for 30 nm ceria ENM were n = 6 for al times except 1, 20 168 and 720 h where n = 10, 8, 3 and 11; and for the 55 nm ceria ENM were n = 10 and 7 at 1 and 20 h, respectively. The horizontal line at the top of each graph shows the calculated cerium concentration in blood representing 100% of the dose.

Figure 3. The ratio of Ce concentration in whole blood following iv infusion of 5-, 15-, 30- and 55-nm ceria ENMs from 0.167 to 4 h after their infusion, compared to the cerum ion concentration. Each symbol represents a different rat.

Figure 4. The ratio of cerium in serum to whole blood (as %), following iv infusion of the cerium ion; 5-, 15-, and 30-nm ceria ENMs; mixture of 30-nm cubic + rod ceria ENMs; and 55-nm ceria ENM. Each symbol shows results from a different rat. For the 15-nm ceria ENM the solid curve is the model for the rat shown by the open circle, dashed line

for rat shown by the closed square, and double curve for rat shown by the closed diamond. For the 30-nm ceria ENM the solid curve is the model for the rat shown by the closed square, dashed line for rat shown by the open circle, double curve for rat shown by the closed diamond, and long dash dot curve for rat shown by the open triangle.

Figure 1

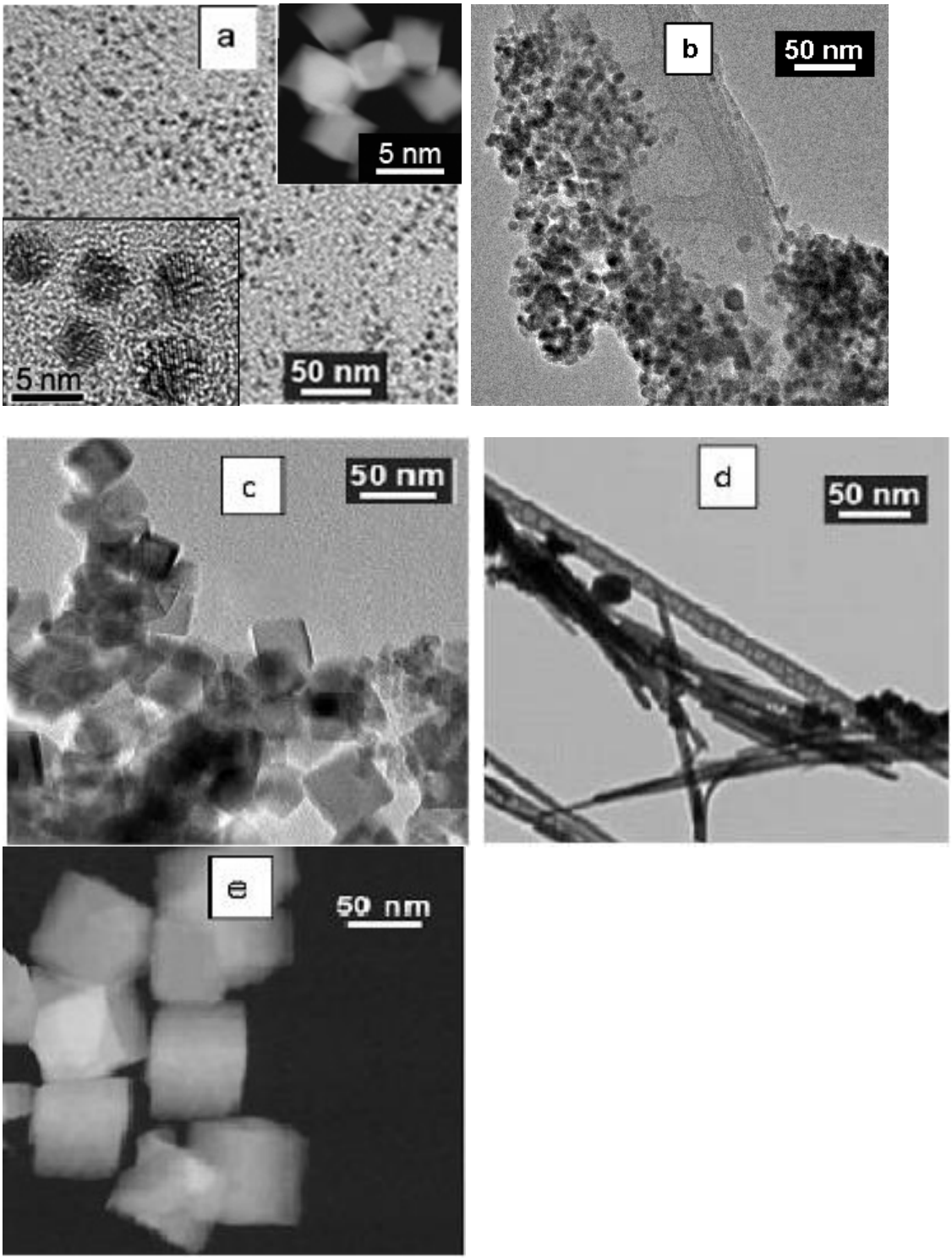

Figure 2.

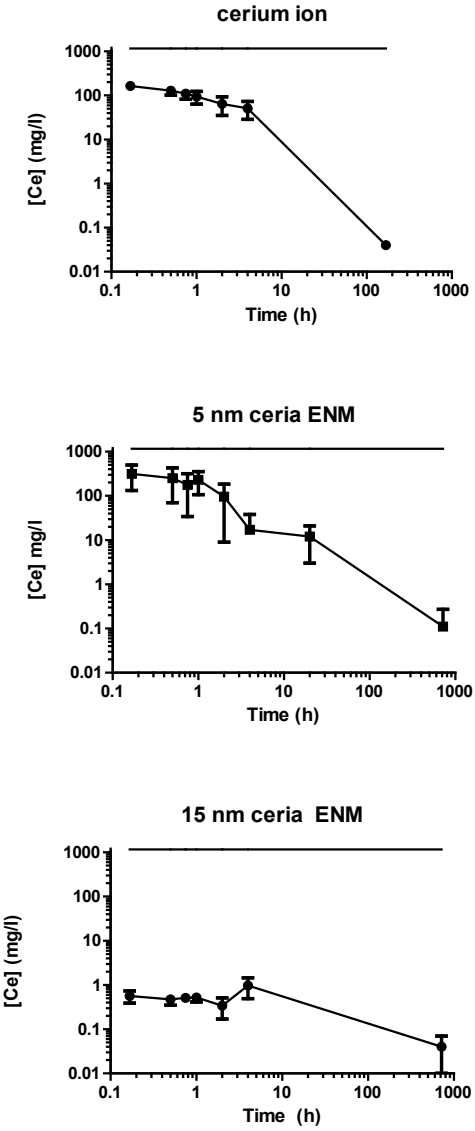
cerium ion
[Ce] (mg/l)
1000
100
10
1
0.1
0.01
0.1
1
10
100
1000
Time (h)
5 nm ceria ENM
[Ce] mg/l
1000
100
10
1
0.1
0.01
0.1
1
10
100
1000
Time (h)
15 nm ceria ENM
[Ce] (mg/l)
1000
100
10
1
0.1
0.01
0.1
1
10
100
1000
Time (h)

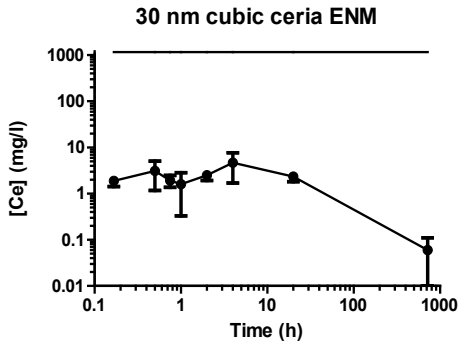
30 nm cubic ceria ENM
[Ce] (mg/l)
1000
100
10
1
0.1
0.01
0.1
1
10
100
1000
Time (h)

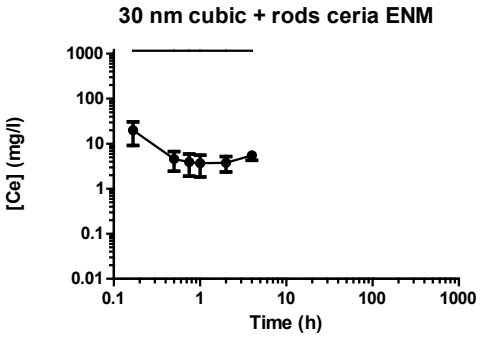
30 nm cubic + rods ceria ENM
[Ce] (mg/l)
1000
100
10
1
0.1
0.01
0.1
1
10
100
1000
Time (h)

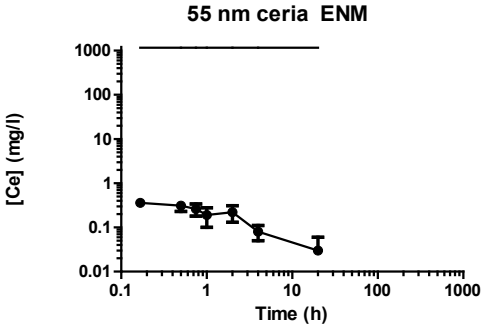
55 nm ceria ENM
[Ce] (mg/l)
1000
100
10
1
0.1
0.01
0.1
1
10
100
1000
Time (h)

Figure 3.

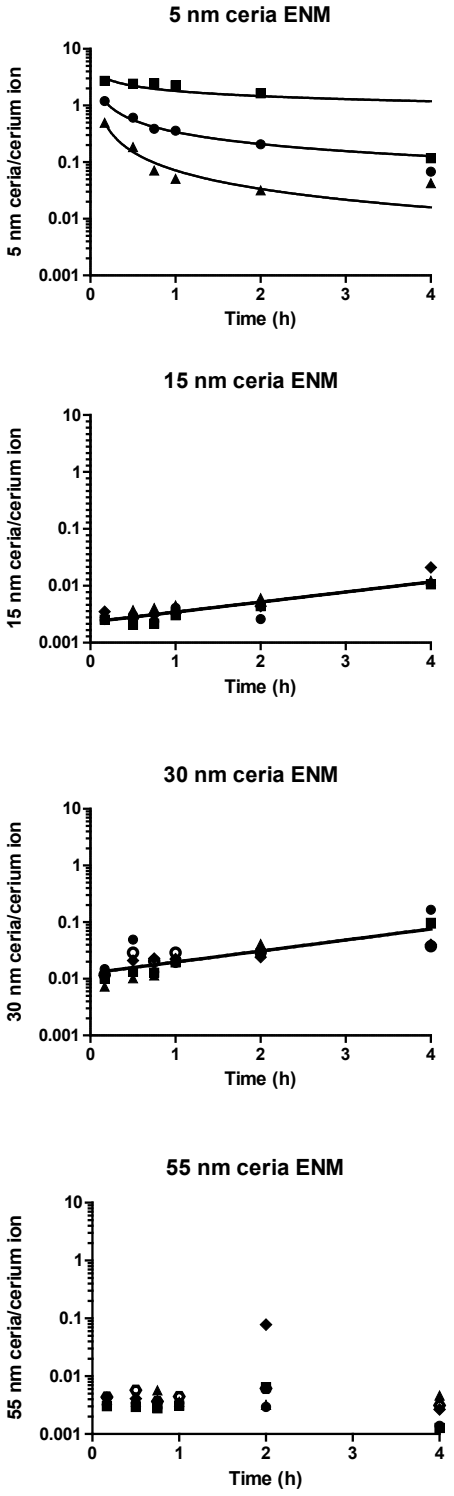
5 nm ceria ENM
5 nm ceria/cerium ion
Time (h)
15 nm ceria ENM
15 nm ceria/cerium ion
Time (h)
30 nm ceria ENM
30 nm ceria/cerium ion
Time (h)
55 nm ceria ENM
55 nm ceria/cerium ion
Time (h)

Figure 4.

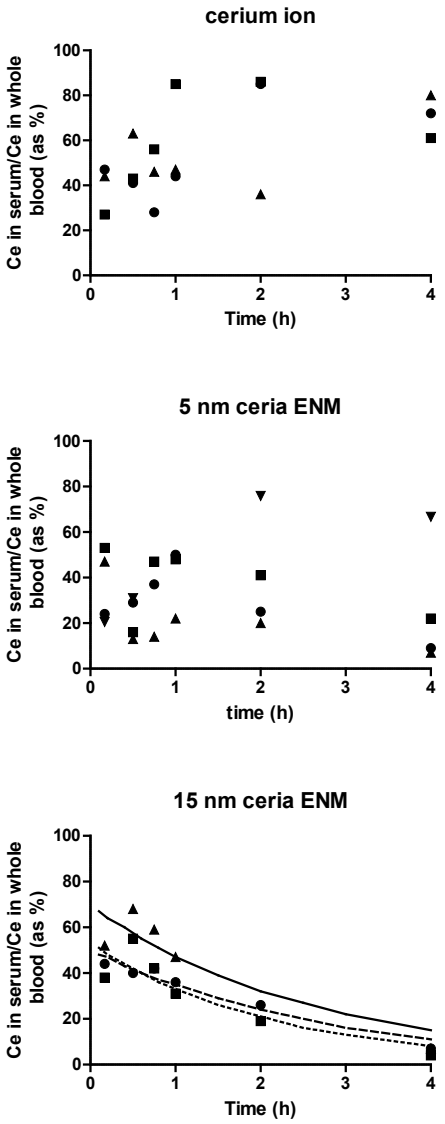
cerium ion
Ce in serum/Ce in whole blood (as %)
Time (h)
5 nm ceria ENM
Ce in serum/Ce in whole blood (as %)
time (h)
15 nm ceria ENM
Ce in serum/Ce in whole blood (as %)
Time (h)

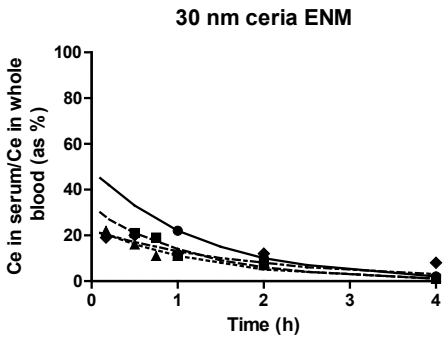
30 nm ceria ENM
Ce in serum/Ce in whole blood (as %)
100
80
60
40
20
0
0
1
2
3
4
Time (h)

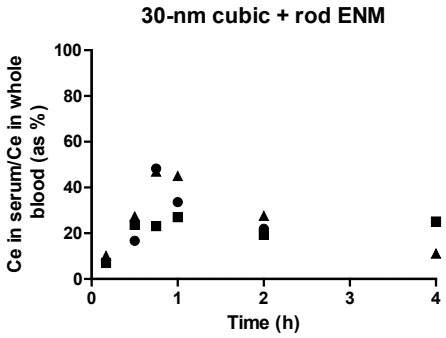
30-nm cubic + rod ENM
Ce in serum/Ce in whole blood (as %)
100
80
60
40
20
0
0
1
2
3
4
Time (h)

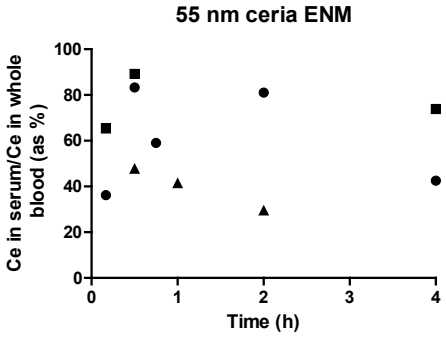
55 nm ceria ENM
Ce in serum/Ce in whole blood (as %)
100
80
60
40
20
0
0
1
2
3
4
Time (h)

Table 1. Physico-chemical properties of the ceria ENMs. Shape delineation based on TEM data. D_{ave} (average primary particle diameter from number frequency distribution) and standard deviation based on TEM measurements of diameter fitted using lognormal distribution models. Citrate loading expressed as % of monolayer coverage (TGA analysis).

Ceria ENM primary size(nm)	**shape**	**D_{ave}, nm (st. dev.) [TEM, Lognormal model]**	**zeta potential in water at pH~ 7.3 (mV)**	**extent of surface citrate coating**
5	polyhedral	4.6 (0.135)	- 53 ± 7	~ 40%
15	polyhedral	12.0 (0.232)	- 57 ± 5	~ 27%
30	cubic	31.2 (0.478)	- 56 ± 8	~ 18%
55	polyhedral	55 (0.162)	- 32 ± 2*	~ 15%*

* Determinations made on a batch similarly-prepared to that administered to the rats.

Table 2. Pharmacokinetic parameters for the cerium ion; 5-, 15-, 30- and 55-nm ceria ENMs; and mixture of 30-nm cubic and rod ceria ENMs and after iv infusion to rats. Values are means ± SD, calculated from results obtained from times shown (after completion of the infusion).

Parameter	0.167 h to 7 days	0.167 h to 30 days			0.167 to 4 h	
	cerium ion (n=3)	5-nm ceria (n=3)	15-nm ceria (n=4)	30-nm cubic ceria (n=5)	30-nm cubic + rods ceria (n=5)	55 nm ceria (n=5)
			Non-compartmental Analysis			
AUC (h* mg/L)	326 ± 102[a]	2264 ± 1284[b]	361 ± 130[a]	2201 ± 1314[b]	25 ± 8[a]	1.5 ± 0.5[a]
C_{max} (mg/L)	163 ± 27[a]	278 ± 215[b]	0.95 ± 0.34[a]	6.5 ± 3.1[a]	20 ± 11[a]	0.78 ± 0.12[a]
$t_{1/2}$ (h)	2.7 ± 0.8[a]	80 ± 25[b]	-	-	26 ± 36[a]	2.2 ± 0.8[a]
MRT (h)	1.5 ± 0.2[a]	7.1 ± 3.0[a]	41 ± 11[b]	15 ± 11[a]	1.6 ± 1.8[a]	1.5 ± 0.1[a]
			Two Compartment Model		One Compartment Model	
AUC (h* mg/L)	1377 ± 416[c]	690 ± 181[a]	152 ± 41[b]	561 ± 256[a]	72 ± 39[b]	1.9 ± 0.7[b]
C_{max} (mg/L)	190 ± 29[a,b]	372 ± 317[a]	0.82 ± 0.45[b]	3.5 ± 1.7[b]	12 ± 5[b]	0.88 ± 0.44[b]
$t_{1/2-\alpha}$ (h)	0.57 ± 0.13	0.44 ± 0.27	2.5 ± 2.6	12 ± 17	4.3 ± 1.8	1.9 ± 0.6
$t_{1/2-\beta}$ (h)	16 ± 3[b]	124 ± 53[a,b]	239 ± 56[c]	140 ± 43[a]	-	-
MRT (h)	21 ± 3[c]	92 ± 53[a,c]	343 ± 83[b]	192 ± 57[a]	6.3 ± 2.6[c]	2.8 ± 0.8[c]
CL (L/h/kg)	0.078 ± 0.028[a]	0.15 ± 0.04[a]	0.71 ± 0.24[a]	0.22 ± 0.11[a]	1.4 ± 1.0[a]	46 ± 30[b]
Vd_{ss} (L/kg)	1.7 ± 0.8[a]	15 ± 12[a]	240 ± 8[b]	38 ± 12[a]	9.6 ± 3.9[a]	130 ± 42[c]

AUC, area under the concentration–time curve; $t_{1/2-\alpha}$, first half-life; $t_{1/2-\beta}$, second half-life; C_{max}, peak concentration; CL, Clearance; MRT, mean residence time; Vd_{ss}, volume of distribution at steady state.

* For each parameter, results that do not have the same superscript letters are statistically significantly different by post hoc test ($p < 0.05$).

Table 3. The whole blood compartment model, serum and clot partitioning, and ceria ENM vs. cerium ion ratio results of the six materials studied.

Material	Compartment modeling	$R = \frac{[Ce]_{ceria}}{[Ce]_{cerium(ion)}}$	Serum/whole blood partitioning
Cerium ion	Fits the two compartment model	Not applicable	No strong trend
5 nm ceria	Fits the two compartment model; longer persistence in the second compartment than the cerium ion	Time-dependent reduction in [Ce] relative to the ion; 1st order or other process possible	No strong trend
15 nm ceria	Rapid loss during infusion; Apparent re-distribution to blood in 2-4 hours	Increase relative to $[Ce]_{ion}$; 1st order process	Reduction in serum levels with time; 1st order process (opsonization ?)
30 nm ceria	Rapid loss during infusion; Apparent re-distribution to blood in 2-4 hours	Increase relative to $[Ce]_{ion}$; 1st order process	Reduction in serum levels with time; 1st order process (opsonization ?)
Cubic + rod ceria	Loss during infusion; Apparent redistribution to blood in 2-4 hours	No strong trend	No strong trend; less than 50% in serum
55 nm ceria	Rapid loss during infusion; No apparent re-distribution to whole blood in 2-4 hours	No strong trend	No strong trend